Poly(ethylene oxide-*b*-isoprene) Diblock Copolymer Phase Diagram

G. Floudas,*,† B. Vazaiou,‡ F. Schipper,† R. Ulrich,§ U. Wiesner,§ H. Iatrou,‡ and N. Hadjichristidis‡

Institute of Electronic Structure and Laser, Foundation for Research and Technology-Hellas (FO.R.T.H.), P.O. Box 1527, 711 10 Heraklion, Crete, Greece; Department of Chemistry, University of Athens, Zografou 15771, Athens, Greece; and Max-Planck Institut für Polymerforschung, Postfach 3148, D-55021 Mainz, Germany

Received November 15, 2000; Revised Manuscript Received January 30, 2001

ABSTRACT: The phase state of 25 poly(ethylene oxide-*b*-isoprene) (PEO−PI) diblock copolymers spanning the composition range $0.05 < f_{PEO} < 0.8$ has been studied using small-angle X-ray scattering and rheology. In addition, the thermal and thermodynamic properties have been obtained from differential scanning calorimetry and pressure−volume−temperature measurements. Twenty of the diblocks exhibit at least one order-to-order transition, and two show four ordered phases. The phase diagram consists of four equilibrium phases in the melt; lamellar (Lam), hexagonally packed cylinders (Hex), spheres packed in a body centered cubic lattice (bcc) and a bicontinuous cubic phase with the $Ia\bar{3}d$ space group symmetry known as the gyroid phase. The latter is formed for the range of compositions $0.4 < f_{PEO} < 0.45$ which are the highest ever reported for a stable gyroid phase. The high asymmetry in the present phase diagram is attributed to the high conformational asymmetry of the PEO and PI ($\epsilon = 2.72$). At low temperatures, upon PEO crystallization, all phases revert to the crystalline lamellar structure (L_c). Within the composition range $0.66 < f_{PEO} < 0.7$ another intermediate phase is formed known as perforated layers (PL) which is clearly not an equilibrium phase. The thermal expansion coefficient was found to be a sensitive probe of the ordered microstructures.

I. Introduction

Block copolymer polymorphism has been the subject of intense theoretical and experimental work over the last 20 years.[1−3] Within Leibler's mean-field theory[4] (MFT), two parameters χN and f, dictate the block copolymer phase behavior, where χ is the Flory−Huggins segment−segment interaction parameter, N is the degree of polymerization, and f is the block copolymer composition. The product χN determines the degree of segregation of the blocks. When $\chi N \leq 10$, entropic terms dominate resulting in a disordered (Dis) phase. When $\chi N > 10$, enthalpic terms dominate causing an order-to-disorder (ODT) transition where the unlike segments segregate into a variety of ordered periodic microstructures. For nearly symmetric compositions, the unlike blocks form domains composed of alternating layers, known as the lamellar (Lam) phase. A composition slightly off-symmetry results in the formation of another layered structure where the minority component layers are interrupted by channels through which the majority component layers are connected.[5] The structure is known as perforated layers (PL) and despite earlier assignment as an equilibrium phase is now known to be a long-lived metastable state.[6,7] In the vicinity of the PL phase, another complex phase is formed. This phase is a bicontinuous structure with $Ia\bar{3}d$ space group symmetry, with the minority component forming two interpenetrating 3-fold coordinated networks, known as the gyroid phase.[8] For more asymmetric compositions a hexagonal phase (Hex) is formed when the minority component forms hexagonally packed cylinders and a spherical phase (bcc) when the minority component forms spheres packed in a body-centered cubic lattice.

Additional factors play a very important role in determining the phase state: copolymer architecture,[9−17] fluctuation effects,[18,19] and conformational asymmetry.[20−22] Copolymer architecture, i.e., the way the blocks are connected, was shown to have a strong influence on the phase behavior by shifting the order-to-disorder transition temperatures and the boundaries between ordered phases.[9−14] Fluctuation effects scale as $\bar{N}^{-1/3}$, where $\bar{N} = (\alpha^6/u^2)N$, and α and u are the statistical segment length and volume, respectively, and raise the T_{ODT} and allow for direct transitions between the different ordered phases and the disordered phase.[15] The theory was developed by Fredrickson and Helfand by applying a concept originally introduced by Brazovskii to the mean-field theory of Leibler. The Fredrickson-Helfand theory, for a compositionally symmetric diblock, predicts an order-to-disorder transition:[18]

$$(\chi N)_{ODT} = 10.5 + \frac{41}{\bar{N}^{1/3}} \quad (1)$$

The theory correctly predicts the shift of the phase diagram as observed experimentally, however, the correction term is meaningful only for very high molecular weights which are normally higher than the experimental ones (i.e., $\bar{N} > 10^4$).

Recent self-consistent field theory calculations[20−22] suggested that conformational asymmetry plays a dominant role on the order-to-disorder and order-to-order phase boundaries. The main effect of conformational asymmetry is to shift the phase boundaries toward

* Author for correspondence.
† Foundation for Research and Technology-Hellas (FORTH).
‡ University of Athens.
§ Max-Planck Institut für Polymerforschung.

10.1021/ma001957p CCC: $20.00
Published on Web 03/27/2001

compositions richer in the segments with the higher asymmetry.[22] This asymmetry has been attributed to differences in monomer volume and backbone flexibilities of the blocks leading to an overall conformational asymmetry described by the ratio $\epsilon = (\alpha^2_A/u_A)/(\alpha^2_B/u_B)$.[23] Experimental phase diagrams based on poly(isoprene-*b*-styrene) (PI−PS)[5,41] and poly(ethylene-*b*-ethyl ethylene) (PE−PEE)[23−25] were found to be asymmetric and shifted toward the more asymmetric block, thus being in qualitative agreement with the theoretical predictions.

In our earlier investigation, we reported on the phase state of a new system, poly(ethylene oxide-*b*-isoprene) (PEO−PI) rich in PI.[26] We found multiple ordered state transitions and explored the kinetics[27] of the Hex to gyroid transformation using synchrotron SAXS and rheology. In this latter study,[27] we were able to identify the epitaxy, time scales, and, for the first time, the activation barrier of the transformation. In the present study, we report on the complete phase behavior of the PEO−PI system by employing 25 diblock copolymers spanning the composition range from 0.05 to 0.8 with small-angle X-ray scattering (SAXS), rheology, differential scanning calorimetry (DSC), and pressure−volume−temperature (*PVT*) measurements.

The PEO−PI system is a unique system for such an investigation. First, the high interaction parameter facilitates a study of the rich polymorphism with unentangled or lightly entangled chains.[36] For example, a sample with $f_{PEO} = 0.77$ and molecular weight of about 10^4 exhibits five phases within about 200 K. Second, the large difference in electron density between PEO and PI gives rise to sufficient scattering contrast even for very short time intervals. Third, both PEO and PI have the same glass transition temperature (∼200 K) and therefore similar mobilities within the microphase. The latter facilitates kinetic studies in the absence of vitrification. Last, the extreme conformational asymmetry of PEO and PI is expected to affect the phase behavior. In accord with this expectation, the obtained phase diagram is the most asymmetric reported so far for a linear diblock copolymer system. Furthermore, the *PVT* study revealed that the differently ordered phases have different thermal expansion coefficients.

II. Experimental Section

The molecular characteristics of all 25 copolymers are given in Table 1. Fifteen of the diblock copolymers have been synthesized with the procedure described elsewhere.[26] For the remaining copolymers, the following procedure was employed.

Materials. The purification of isoprene (I) (Aldrich) and benzene to the standards required for anionic polymerization has been described in detail elsewhere.[28] The initiator was secondary butyllithium (*sec*-BuLi), which was prepared in a vacuum from *sec*-butyl chloride and lithium dispersion. Ethylene oxide (EO) was purified by condensing an appropriate amount in a flask containing CaH_2. The monomer was stirred for 2 h and was distilled in another flask containing *n*-BuLi. During its exposure to *n*-BuLi, EO was kept at 273 K under stirring for 30 min. This step was repeated twice using new *n*-BuLi each time. Finally the pure monomer was distilled into graduated ampules and stored at 253 K until needed. The solution of *tert*-butyl phosphazene (*t*-BuP_4) used for the polymerizations was prepared as following: an appropriate amount of 1 M in hexane (Fluka) solution of the base was introduced in an apparatus equipped with ampules. The hexane was distilled off and was left overnight in high vacuum to dryness. Then purified hexane was distilled into the apparatus, which was sealed off from the vacuum line, and the solution of *t*-BuP_4 (∼0.5 M) was subdivided into ampules.

Polymerization. The basic reactions used for the synthesis of the PEO−PI diblock copolymers are the following:

$$\text{I} + \textit{sec}\text{-BuLi} \xrightarrow{\text{benzene, 25 °C}} \text{PILi}$$

$$\text{PILi} + \text{EO} \rightarrow \text{PICH}_2\text{CH}_2\text{OLi} \xrightarrow{t\text{-BuP}_4} \text{PI−PEOLi} \xrightarrow{\text{MeOH}} \text{PI−PEO}$$

Esswein et al.[29] found that EO can be polymerized by C−OLi group in the presence of a strong base such as *t*-BuP_4. They concluded that the strong base not only disrupts the aggregates of O−Li but also creates free anions, which are capable to polymerize EO. Förster et al.[30] by using this approach prepared a series of polybutadiene-*b*-PEO block copolymers in THF. However, due to the presence of THF and *t*-BuP_4, the microstructure of the butadiene precursor exhibited 89% 1,2-addition.

In this work, the synthetic approach involved first the polymerization of isoprene in benzene giving the usual 1,4 microstructure, followed by the addition of EO and *t*-BuP_4, (1,05:1,00 ratio to *sec*-BuLi). The polymerization was left for 3 days at 323 K. The living block copolymer was terminated by methanol. The final copolymer was precipitated in cold (253 K) acetone and dried under vacuum to constant weight.

Characterization. Diblock copolymers were characterized by size exclusion chromatography (SEC), ^{1}H NMR and membrane osmometry. The PI precursors were characterized by SEC and low-angle laser light scattering (LALLS). The compositions calculated by the arm and total molecular weights agreed rather well with the compositions obtained by ^{1}H NMR spectroscopy (Table 1). SEC experiments were carried out at 303 K using a Waters 610 pump, Waters model 410 differential refractometer 996 diode-array UV detector, and six columns with a porosity range of 10^2-10^6 Å and a flow rate of 1 mL/min. THF was the carrier solvent. The number-average molecular weight (M_n) of the diblocks were measured with a Jupiter model 231 recording membrane osmometer (MO) at 310 K. Toluene, distilled over CaH_2, was the solvent. The M_n values from MO were obtained from the corresponding $(\pi/C)^{1/2}$ vs C plots where π is the osmotic pressure and C is the concentration. In all cases the correlation coefficient was better than 0,99. The weight-average molecular weight M_w of the PI was measured with a Chromatix KMX-6 low-angle laser photometer. This instrument is equipped with a helium−neon laser and operates at a wavelength of 633 nm. THF, purified over sodium and distilled prior to use, was the solvent at 298 K. The refractive index increments dn/dc in THF at 298 K were measured with a Chromatix KMX-16 refractometer operating at 633 nm and calibrated with aqueous NaCl solutions. In all cases the M_w values were obtained from $(Kc/\Delta R_\theta)^{1/2}$ vs c plots (ΔR_θ, excess Rayleigh ratio; K, combination of known optical and instrument constants; c, concentration). In all cases the correlation coefficient was better than 0.99.

Over a narrow range of molecular weights ($7000 < M_n < 12000$), the phosphazene method yields copolymers with low polydispersity. This is supported by the SEC chromatograms of the PI precursor (Figure 1a) and of the final copolymer (Figure 1b).

Pressure−Volume−Temperature (*PVT*) Measurements. *PVT* measurements were performed on the PEO−PI 7−3 copolymer with a pressure dilatometer (GNOMIX) and for pressure intervals of 10 MPa from 0.1 up to 60 MPa. Specific volume changes (ΔV) were recorded isothermally in the temperature range from 300 to 560 K with a stability of ±0.2 K with an effective heating rate of 0.2 K/min. In another experiment, data were collected under isobaric conditions ($P = 0.1$ MPa) on heating and subsequent cooling. Figure 2 shows the relative changes in the specific volume taken under isothermal conditions for the different pressures. The result from the isobaric experiment is shown in the inset. Using the ln V vs T and ln V vs P representations we have calculated, respectively, the thermal expansion coefficient $\alpha_P = (\partial \ln V/\partial T)_P$ and the isothermal compressibility $b_T = -(\partial[\ln V]/\partial P)_T$ and

Table 1. Molecular Characteristics and Phase State of the Diblock Copolymers

sample	$M_{n\,(PI)}$[a]	$M_{n\,(PEO)}$[b]	$M_{n\,(total)}$[c]	M_w/M_n[d]	% wt PI[e]	f_{PEO}[f]	phase state (transition temp in K)
PEO−PI 7−77	77 400	6700	84 100	1.05	0.92	0.06	bcc at 333 K
PEO−PI 1−11	10 600	1200	11 800	1.05	0.90	0.08	$L_c \xrightarrow{311}$ bcc
PEO−PI 1−10	9700	1200	10 900	1.09	0.90	0.09	bcc at 333 K
PEO−PI 2−12	12 400	1800	14 200	1.06	0.87	0.1	$L_c \xrightarrow{315}$ bcc
PEO−PI 2−13	13 140	2000	15 140	1.06	0.87	0.11	bcc at 333 K
PEO−PI 3−12	12 400	2900	15 300	1.05	0.81	0.156	$L_c \xrightarrow{318}$ bcc
PEO−PI 1−5	5400	1200	6600	1.05	0.81	0.16	bcc $\xrightarrow{308}$ Dis
PEO−PI 4−11	10 600	4300	14 900	1.07	0.71	0.24	$L_c \xrightarrow{331}$ Hex
PEO−PI 6−10	10 200	6200	16 400	1.05	0.62	0.32	$L_c \xrightarrow{325}$ Hex
PEO−PI 4−6	6500	4300	10 800	1.05	0.60	0.34	$L_c \xrightarrow{325}$ Hex
PEO−PI 4−5	5400	4400	9800	1.08	0.55	0.39	$L_c \xrightarrow{325}$ Hex $\xrightarrow{418}$ Gyroid $\xrightarrow{486}$ Dis
PEO−PI 5−5	5400	5000	10 400	1.04	0.49	0.45	$L_c \xrightarrow{323}$ Hex $\xrightarrow{393}$ Gyroid $\xrightarrow{503}$ Dis
PEO−PI 5−3	3450[g]	5200	8600[h]	1.02	0.40	0.55	$L_c \xrightarrow{328}$ Lam − up to 493 K
PEO−PI 6−4	3400	6000	9400	1.09	0.36	0.59	$L_c \xrightarrow{331}$ Lam
PEO−PI 5−3	2750[g]	5000	7800[h]	1.02	0.36	0.594	$L_c \xrightarrow{328}$ Lam − up to 453 K
PEO−PI 5−3	3100[g]	5000	8300[h]	1.02	0.35	0.596	$L_c \xrightarrow{328}$ Lam − up to 493 K
PEO−PI 20−11	10 600	19 700	30 300	1.12	0.35	0.596	$L_c \xrightarrow{344}$ Lam
PEO−PI 5−2	2250[g]	5200	7400[h]	1.05	0.30	0.65	$L_c \xrightarrow{328}$ Lam $\xrightarrow{488}$ Dis
PEO−PI 6−2	2500[g]	5700	8100[h]	1.02	0.31	0.65	$L_c \xrightarrow{328}$ Lam $\xrightarrow{463}$ Dis
PEO−PI 7−3	2850[g]	7360	10 260[h]	1.01	0.27	0.67	$L_c \xrightarrow{328}$ Lam $\xrightarrow{373}$ PL $\xrightarrow{496}$ Gyroid $\xrightarrow{553}$ Dis
PEO−PI 9−3	3200[g]	8700	12 400[h]	1.01	0.25	0.69	$L_c \xrightarrow{328}$ Lam $\xrightarrow{363}$ PL $\xrightarrow{498}$ Gyroid
PEO−PI 7−2	2150[g]	7100	9200[h]	1.01	0.31	0.728	$L_c \xrightarrow{328}$ Hex $\xrightarrow{515}$ Dis
PEO−PI 21−5	5400	21 000	26 400	1.11	0.205	0.75	$L_c \xrightarrow{325}$ Hex
PEO−PI 7−2	1850[g]	7200	8950[h]	1.01	0.23	0.766	$L_c \xrightarrow{328}$ Hex $\xrightarrow{486}$ Dis
PEO−PI 5−1	940	4600	5400	1.07	0.17	0.79	$L_c \xrightarrow{323}$ Dis

[a] From SEC. [b] From ^{1}H NMR. [c] Calculated as $M_n(\text{total}) = M_n(\text{PI}) + M_n(\text{PEO})$. [d] SEC in THF at 303 K. [e] ^{1}H NMR in $CDCl_3$ at 303 K. [f] Calculated from $N_n^* = N^*_{n,PI} + N^*_{n,PEO} = N_{n,PI}(\rho^*_{EO}/\rho^*_I)^{1/2} + N_{n,PEO}(\rho^*_I/\rho^*_{EO})^{1/2}$, and $f = N^*_{n,PEO}/(N^*_{n,PI} + N^*_{n,PEO})$ where $N_{n,i}$ are the degrees of polymerization of each block and ρ^*_i are the molar densities. For the density, we have used the values 0.895 and 1.12 g/cm^3 for PI and PEO, respectively. [g] LALLS in THF at 303 K. [h] Membrane osmometry in toluene at 308 K.

compared them within different temperatures regimes corresponding to the different phases (see below).

Differential Scanning Calorimetry (DSC). A Polymer Laboratories DSC capable of programmed cyclic temperature runs over the range 113−673 K was used. The samples were first heated from ambient temperature with a rate of 10 K/min. The result from such heating runs are shown in Figure 3 for the PEO−PI 7−3 and the PEO−PI 7−2 copolymers. From the thermograms we obtained the apparent melting temperature of the PEO block from the peak of the endothermal processes. Another endothermal process exists at higher temperatures as a result of mixing at the apparent order-to-disorder transition temperature.

Small-Angle X-ray Scattering (SAXS). An 18kW rotating anode X-ray source (Rigaku) was used with a pinhole collimation and a two-dimensional detector (Siemens) with 512 × 512 pixels. All samples were first heated to their disordered state in an oven and then slowly cooled to room temperature allowing for the crystallization of the PEO block. Measurements of 30 min long were made at intervals of 5 K on heating and subsequent cooling within the range 298−553 K, with a stability better than ±0.2 K using an appropriate computer program. Additional SAXS/WAXS measurements with a higher resolution were made at the X27C beamline of the National Synchrotron Light Source at Brookhaven National Laboratory. The main body of this investigation with respect to the order-

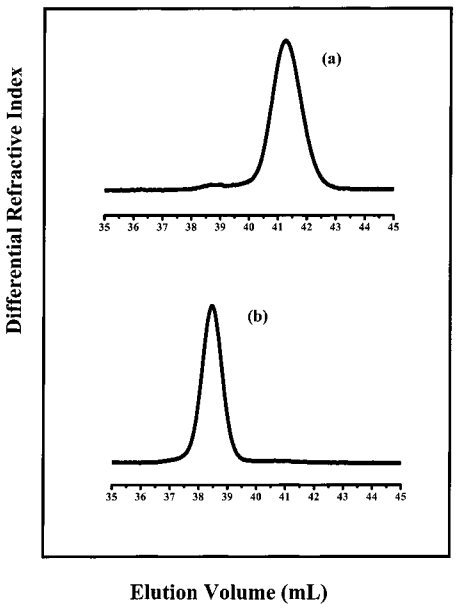

Figure 1. SEC chromatograms of (a) PI and (b) PEO−PI in THF at 303 K.

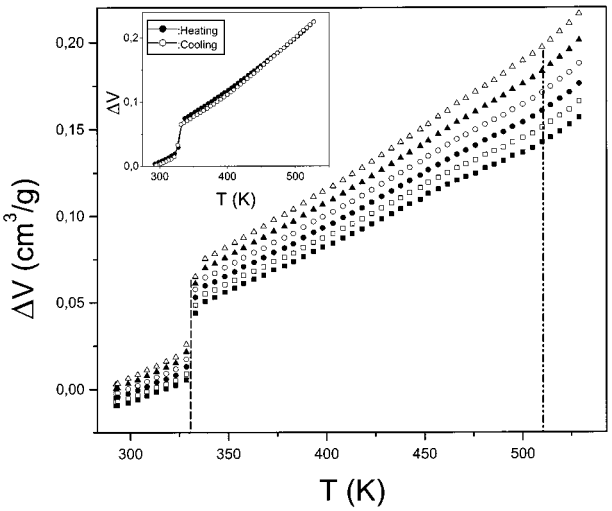

Figure 2. Relative change of specific volume (ΔV) vs temperature from $P-V-T$ measurements for the PEO−PI 7−3 copolymer (sample 20 from Table 1). The different symbols correspond to different applied pressures: (△) $P = 0.1$ MPa, (▲) $P = 10$ MPa, (○) $P = 20$ MPa, (●) $P = 30$ MPa, (□) $P = 40$ MPa, and (■) $P = 50$ MPa. All data were taken under isothermal conditions. The dashed and dash−dotted lines show, respectively, the melting and the order-to-disorder transition temperatures. In the inset, the change of volume is shown during heating (filled symbols) and subsequent cooling (open symbols) under isobaric conditions (at 0.1 MPa). Notice the hysteresis below 470 K.

to-order phase transformations will be the subject of another publication.[31]

Transmission Electron Microscopy (TEM). A Zeiss EM902 electron microscope operated at 80 kV using an objective aperture of 8 mrad was used. Prior to sectioning the PEO−PI 21−5 sample was exposed to OsO_4. Ultrathin sections were produced using a Reichert ultramicrotome. Micrographs were recorded on a Kodak FGRP 35 mm film. Figure 4 provides two TEM images of the contrasted PEO−PI 21−5 sample (top) and of the uncontrasted PEO−PI 20−11 sample (bottom). The image from the PEO−PI 21−5 sample ($f_{PEO} = 0.75$) show the formation of cylinders of the stained (PI) block. Notice the gradient from the edge of the cylinders to the interior which is probably caused by the inhomogeneous penetration of the

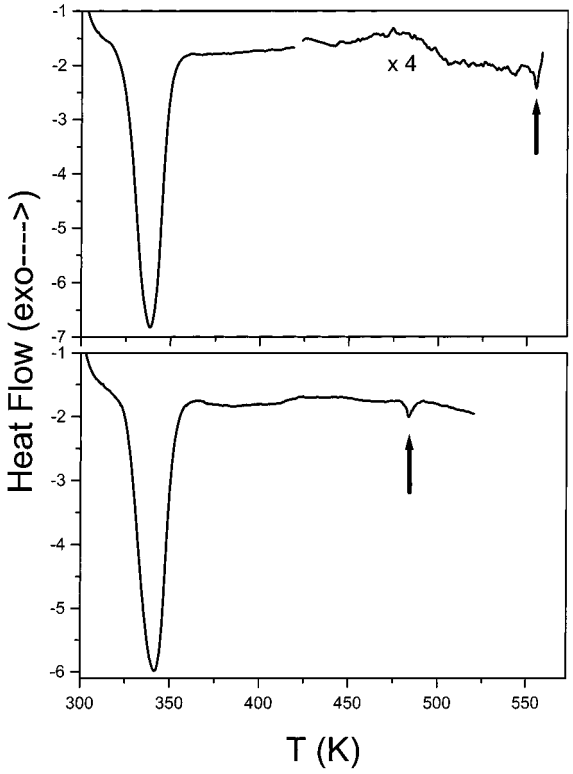

Figure 3. Heat flow obtained during heating for the PEO−PI 7−3 (top) (sample 20 from Table 1) and the PEO−PI 7−2 copolymer (bottom) (sample 24 from Table 1). Notice the strong endothermic peak at the melting of the semicrystalline PEO and the much smaller endothermic peaks (indicated by arrows) associated with the order-to-disorder transition temperatures.

contrasting agent. The image from the PEO−PI 20−11 copolymer ($f_{PEO} = 0.596$) was taken from a sample cooled from above the PEO melting temperature to the crystalline lamellar phase and show that the PI lamellae (bright areas) are perforated by the PEO (dark areas).

Rheology. An advanced rheometric expansion system (ARES) equipped with a force-rebalanced transducer was used in the oscillatory mode. Depending on the sample and T range we have made use of two transducers with 2000, 2 g·cm and 200, 0.2 g·cm upper and lower sensitivity, respectively. The samples were prepared on the lower plate of the 8 or 25 mm diameter parallel plate geometry setup and were heated under a nitrogen atmosphere until they could flow. Subsequently, the upper plate was brought into contact, the gap thickness was adjusted to 1 mm and the sample was slowly cooled to the desired starting temperature. The elastic (G') and loss (G'') moduli were monitored in different types of experiments. First, the linear and nonlinear viscoelastic ranges were identified, by recording the strain amplitude dependence of the complex shear modulus $|G^*|$. In all subsequent experiments, strain amplitudes within the linear viscoelastic range were used (typically below 2%). These experiments involved (i) isochronal temperature scans within the range 298−553 K (heating and cooling) aiming to identify the (apparent) melting temperature of PEO crystals, the order-to-disorder transition temperature T_{ODT}, and possibly an order-to-order transition, (ii) isothermal frequency scans for temperatures in the range 303−553 K and for frequencies $10^{-2} < \omega < 10^2$ rad/s with a strain amplitude below 2%, and (iii) isochronal/isothermal kinetic experiments at $\omega = 1$ rad/s. The latter experiments involved monitoring the order-to-order transformations between the different phases of the PEO−PI 7−3 copolymer, and the results from the combined rheology and synchrotron SAXS experiments on the dynamics of phase transformation will be the subject of a separate publication.[31]

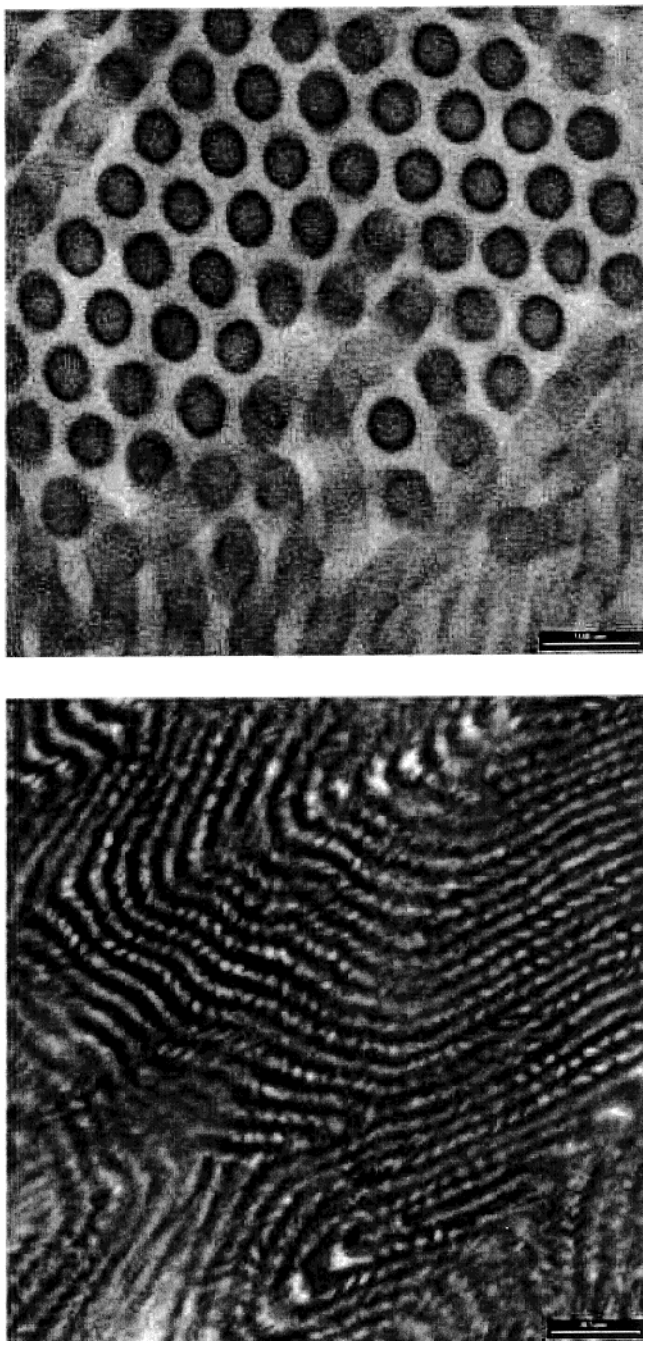

Figure 4. TEM images of the contrasted PEO−PI 21−5 sample (top) and of the uncontrasted PEO−PI 20−11 diblock (bottom).

III. Results and Discussion

Thermal and Thermodynamic Parameters. The *PVT* and DSC curves shown in Figures 2 and 3, respectively, for the PEO−PI 7−3 diblock copolymer reveal a first-order transition at about 328 K with discontinuous changes of the specific volume and a strong endothermic peak associated with the melting of the semicrystalline block (PEO). From the heat of fusion we obtain the crystallinity as $X_c = \Delta H/w_{PEO}\Delta H°$, where w_{PEO} is the PEO weight fraction in the copolymer and $\Delta H°$ is the heat of fusion for a 100% crystalline PEO ($\Delta H° = 200$ J/g).[32] The crystallinity amounts to 60 and 65% for the PEO−PI 7−3 and PEO−PI 7−2 copolymers, respectively. The isothermal *PVT* data of the relative change in specific volume hint toward an additional mechanism at about 515 K, which is manifested by a change in the T dependence rather than by a discontinuity in the specific volume. In addition, in the thermogram of the PEO−PI 7−3 copolymer, at 553 K, there is a weak endothermic peak, with a heat of fusion of about 0.7 J/g, associated with the weak first-order transition from the ordered to the disordered phase (see below). This value for the heat of fusion at the T_{ODT} can be accounted for by $\Delta H = RT_{ODT}f(1 - f)(\chi N)_{ODT}/M_n$,[33,34] where R is the gas constant, N is the degree of polymerization, and M_n is the total number-averaged molecular weight. The difference in the transition temperatures in the two experiments is probably due to the very different heating rates (0.2 vs 10 K/min in *PVT* and DSC, respectively). The small heat of fusion and the relatively weak effect in the specific volume calls for a broad supercooling effect for the order-to-disorder transition which has been documented in the literature for a number of block copolymers. In the intermediate T range, between the two first-order transitions, there are additional changes in the specific volume and heat flow showing hysteresis (inset to Figure 2) and a steplike decrease, respectively. However, no endothermic peak is observed and the steplike decrease at about 490 K (in Figure 3), which as we will see below is in the vicinity of the PL to gyroid transformation, points toward conformational changes rather than to a true thermodynamic phase transition. In conclusion, the *PVT* and DSC spectra revealed two first-order transitions in the PEO−PI 7−3 copolymer; a "strong" one associated with the melting of semicrystalline PEO and a "weak" one associated with the melting of the high T microdomain morphology (gyroid) to the disordered phase. Intermediate transformations may exist (see below), but do not exhibit the characteristics of true first-order transitions.

SAXS. We have used conventional SAXS and rheology to probe the microstructures and the associated viscoelastic properties for all samples shown in Table 1. It is well documented in the literature[6,7,10,13] that the different microstructures of block copolymers have different viscoelastic contrast, which can serve as a fingerprint of the underlying morphology. Figure 5 displays the storage modulus of the PEO−PI 7−2 copolymer on heating (heating rate of 2 K/min), with $\omega = 1$ rad/s and with a low strain amplitude (<0.5%). The modulus displays different regimes: below 323 K the modulus exhibits the highest values as a result of the PEO crystals in the lamellar morphology. The SAXS pattern taken at 323 K shows broad reflections with relative positions 1:2 which is characteristic of a crystalline lamellar structure (L_c) with a broad distribution of crystal sizes. At 328 K, the PEO crystals melt to another microstructure composed of cylinders of the minority phase with hexagonal packing (reflections with relative positions at $1:3^{1/2}:7^{1/2}:9^{1/2}$). At 486 K this microstructure "melts" at the apparent order-to-disorder transition temperature (the equilibrium T_{ODT}^0 is located a few degrees higher[35]) which is shown by the drop of the storage modulus and by the broad liquidlike structure factor.

Figure 6 gives some representative SAXS spectra of the PEO−PI 7−3 diblock copolymer at four temperatures corresponding to the different ordered morphologies. Starting from low temperatures, at 328 K, the spectrum shows broad reflections with relative positions 1:2 indicative of the formation of the crystalline lamellar

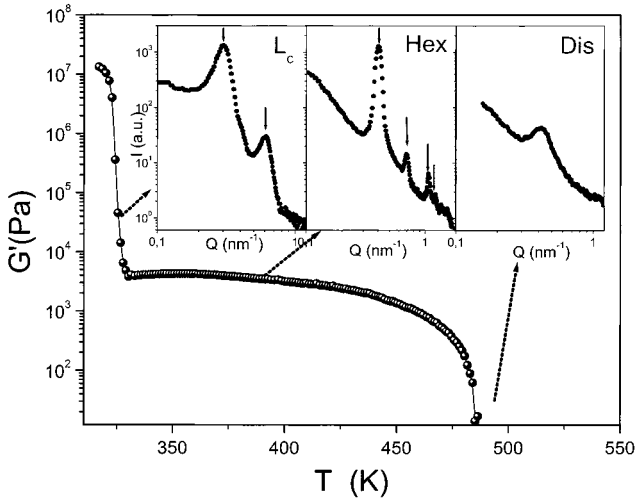

Figure 5. Temperature dependence of the storage modulus obtained on heating the PEO−PI 7−2 copolymer (sample 24 from Table 1) with a heating rate of 2 K/min and a strain amplitude of below 1%. The precipitous drops of the modulus at 328 and 486 K signify, respectively, the melting and order-to-disorder transition temperatures. Representative SAXS spectra are shown as insets at three temperatures: 323 K (left), $T = 393$ K (center), and $T = 493$ K (right). The arrows indicate positions of the main and higher order peaks corresponding to the crystalline lamellar ($T = 323$ K) and hexagonal arrangement of cylinders ($T = 393$ K). The spectrum at $T = 493$ K is characteristic of the disordered regime.

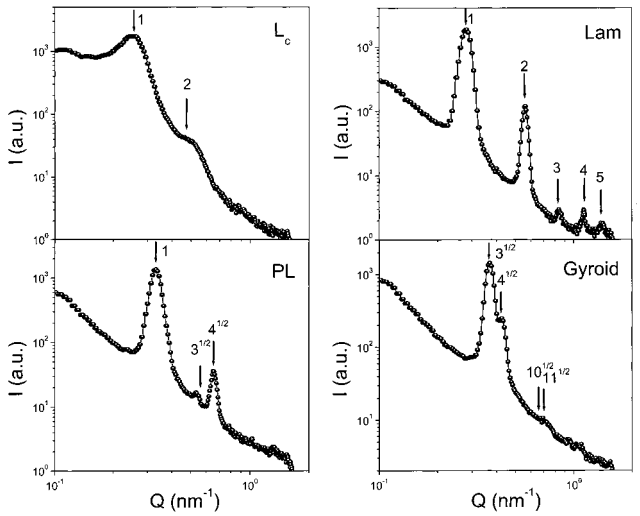

Figure 6. Representative SAXS spectra for the PEO−PI 7−3 copolymer (sample 20 from Table 1) shown at different temperatures corresponding to different microstructures. Arrows indicate positions of the main and higher order peaks with relative positions 1:2 ($T = 328$ K − L_c), 1:2:3:4:5 ($T = 338$ K − Lam), $1:3^{1/2}:4^{1/2}$ ($T = 433$ K − PL), and $3^{1/2}:4^{1/2}:11^{1/2}$ ($T = 493$ K− gyroid).

structure (L_c). Upon melting, the spectrum shown at 338 K, depicts reflections with relative positions 1:2:3:4:5 corresponding to an amorphous lamellar (Lam) structure. By subsequent heating the spectra undergo further changes; the main peak at Q^* broadens, and the second-order reflection, corresponding to the Lam structure, loses intensity. In addition, another weak reflection appears with a position approximately $3^{1/2}$ relative to the main peak. This intermediate structure has been identified as perforated layers (PL) composed of channels of the majority component layers which form a monocontinuous structure. The structure has both 3-fold coordinated domains and a layered geometry thus

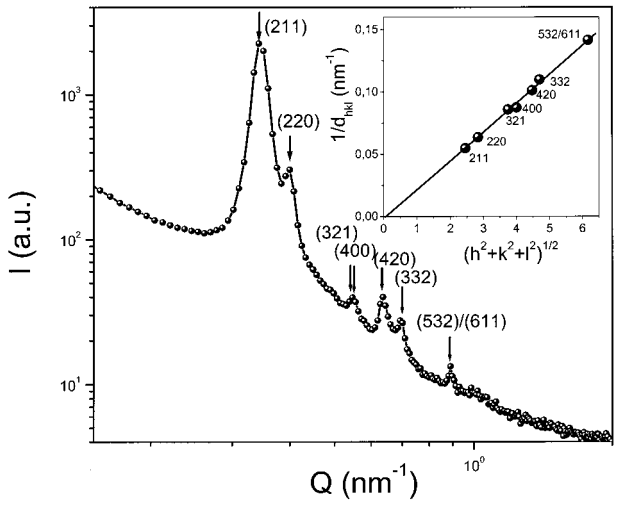

Figure 7. High-resolution SAXS spectrum of the PEO−PI 3−7 copolymer taken at 483 K. Seven Bragg peaks are identified with arrows which can be indexed as the (211), (220), (321), (400) (420) (332), and (532)/(611) reflections of the bicontinuous cubic phase with the $I\alpha\bar{3}d$ symmetry (gyroid). In the inset the reciprocal d spacings of the marked reflections are plotted vs $(h^2 + k^2 + l^2)^{1/2}$, showing the validity of the crystallographic space group assignment.

combining elements from the gyroid and lamellar structures. The SAXS spectrum at 433 K shows that the PL phase lacks long-range order and its identification by SAXS alone is not unique (see below). By heating, the system undergoes another transition to a microstructure with peaks at relative positions $3^{1/2}:4^{1/2}:10^{1/2}:11^{1/2}$. To aid in the identification of this microdomain morphology we have employed high-resolution SAXS measurements on the same sample.

The high-resolution synchrotron SAXS pattern obtained at 483 K is shown in Figure 7. A total of seven Bragg peaks are identified (marked with arrows) which can be indexed as the (hkl) reflections (211), (220), (321), (400), (420), (332) and (532)/(631) of the bicontinuous cubic phase with symmetry $I\alpha\bar{3}d$. The latter space group has the following Bragg reflections:[8] (211), (220), (321), (400), (420), (332), (422), (431), (521), (440), (532)/(631), which gives peaks with relative positions $6^{1/2}$: $8^{1/2}$:$14^{1/2}$: $16^{1/2}$: $20^{1/2}$: $22^{1/2}$:$24^{1/2}$: $26^{1/2}$: $30^{1/2}$: $32^{1/2}$: $38^{1/2}$, and the seven reflections of the diblock shown in Figure 7 are in good agreement with most of the above. In the inset, the reciprocal d spacings ($1/d_{hkl}$) of the marked reflections are plotted vs $(h^2 + k^2 + l^2)^{1/2}$ and the line with zero intercept shows the validity of the crystallographic space group assignment.

Rheology. The SAXS measurements have identified four ordered microdomain morphologies in the PEO−PI 7−3 copolymer, namely, L_c, Lam, PL, and gyroid, but the assignment of the PL phase from SAXS in unoriented samples is not unique. However, rheology provides a useful tool of distinguishing between the ordered microstructures based on the difference in elasticity of the various phases. In a previous study of the PEO−PI 4−5 copolymer with the following succession of phases, L_c−Hex−gyroid−Dis, the different phases could be arranged according to their elasticity as follows: L_c > gyroid > Hex. For the samples PEO−PI 7−3 and PEO−PI 9−3, the expectation is that, for the four ordered phases, the arrangement would be L_c > gyroid > PL > Lam. This expectation is born out from the bicontinuous and monocontinuous nature of the gyroid

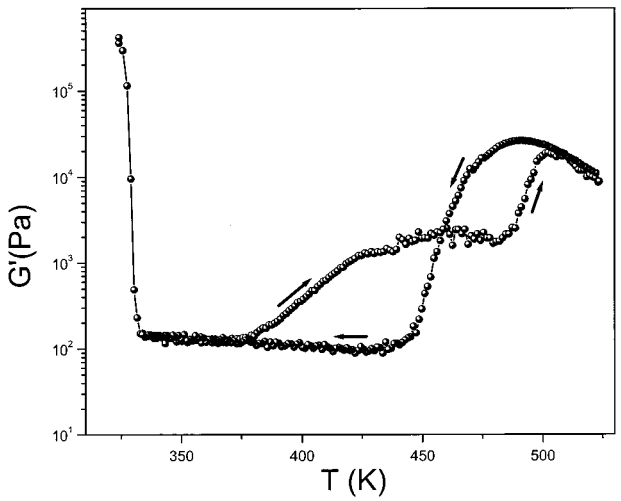

Figure 8. Temperature dependence of the storage modulus for the PEO−PI 7−3 copolymer (sample 20 from Table 1) obtained at 1 rad/s with a low strain amplitude below 1% obtained on heating and subsequent cooling with a rate of 2 K/min. Notice the hysteresis within the *T* range 375−500 K.

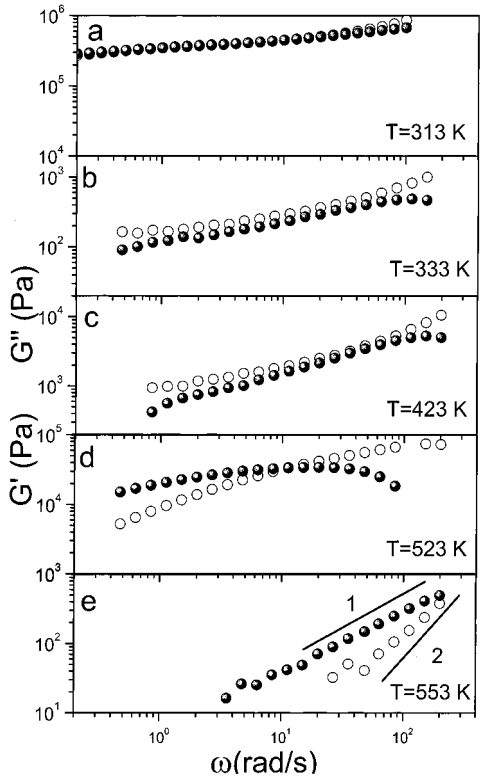

Figure 9. Frequency dependence of the storage (open symbols) and loss (filled symbols) moduli obtained during the heating of the PEO−PI 7−3 copolymer, shown at five temperatures corresponding to the different phases: (a) $T = 313$ K (L_c), (b) $T = 333$ K (Lam), (c) $T = 423$ K (PL), (d) $T = 523$ K (gyroid), and (e) $T = 553$ K (disordered). The strain amplitude in all but the highest temperature was below 1%.

and PL phases, respectively. The elasticity of the L_c phase is expected to be even higher, not for connectivity reasons, but from the intrinsically high modulus associated with the PEO crystals within the PEO domains.

The viscoelastic properties of the different phases of the PEO−PI 7−3 copolymer are shown in Figures 8 and 9, below. As expected, the L_c phase has the highest elasticity as a result of the high crystallinity of the semicrystalline PEO block. Heating above 328 K, the

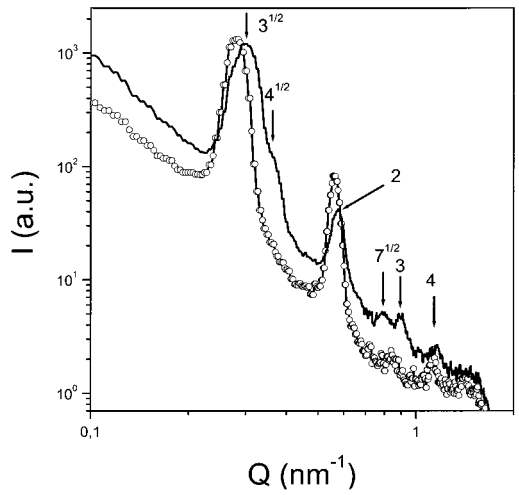

Figure 10. SAXS spectra for the PEO−PI 7−3 copolymer compared at the same temperature ($T = 333$ K) but subjected to different thermal history: (○) spectrum taken during the first heating and the main and higher order peaks with relative positions 1:2:3:4:5 signifying a lamellar structure; (line) spectrum taken during the first cooling from the high-temperature phase (gyroid) with appearance of mixed reflections revealing that the system cools as a Lam and gyroid structure. Notice the different *Q** obtained during the cooling run.

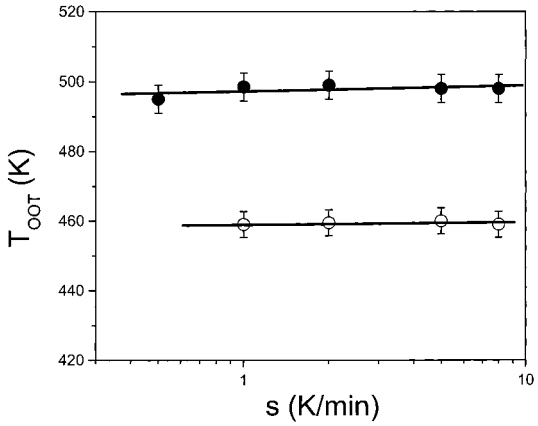

Figure 11. Heating (solid symbols) and cooling (open symbols) rate dependence of the transitions PL−gyroid (heating) and gyroid−Lam (cooling), respectively, obtained from rheology.

system undergoes a first order transition to the "soft" lamellar (Lam) microstructure in excellent agreement with the DSC and *PVT* results. Heating above 375 K, results in the transformation from the Lam to the more elastic PL phase. The Lam to PL transformation is not a sharp transition and as we will see below, the PL phase is not an equilibrium phase. At approximately 490 K, the diblock undergoes a transformation to the $Ia\bar{3}d$/ gyroid phase which, as expected, possess the highest modulus among the ordered amorphous microstructures as a result of the 3-dimensional bicontinuous cubic structure. Despite the high elasticity, the gyroid has peculiar thermal properties, with the sample in many cases having the tendency of flowing out from the rheometer plates. We will discuss this finding later with respect to Figure 12. Cooling from the gyroid phase results in a completely different "path". The modulus drops at about 459 K by 3 orders of magnitude to a value of 10^2 Pa, characteristic of the Lam structure, and at even lower temperatures the PEO starts to crystallize. The isochronal heating and cooling experiments shown

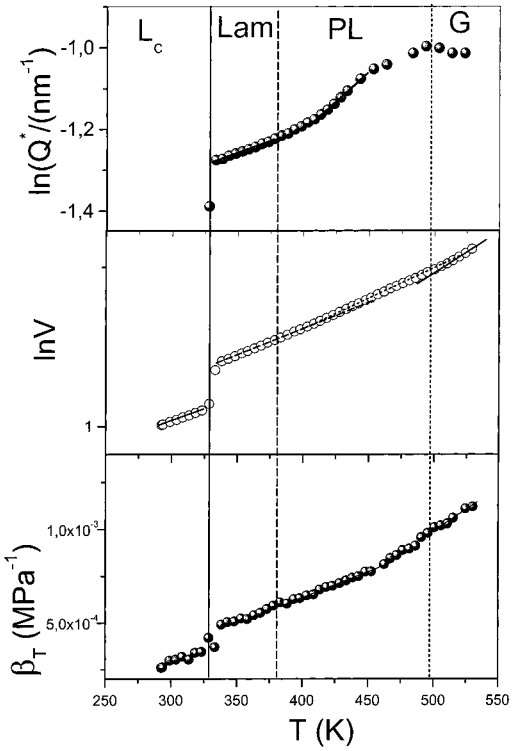

Figure 12. Temperature dependence of ln Q^* (top), of the specific volume (middle), and of the isothermal compressibility (bottom) for the PEO−PI 7−3 copolymer. The vertical lines separate the different phases. Lines give the regimes used in extracting the d(ln Q^*)/dT and of the thermal expansion coefficient of the different microstructures.

in Figure 8 demonstrate that the PL phase is not an equilibrium one; upon cooling the storage modulus bisects the heating curve near the plateau of the PL phase. If the PL phase was formed under equilibrium conditions then it should undercool and show hysteresis. However, only the gyroid phase shows undercooling. We will return to this point later.

Another probe of the viscoelastic contrast between the different microstructures is provided by examining the frequency dependence at selected temperatures. The frequency dependence of the five phases formed by the PEO−PI 7−3 copolymer is shown in Figure 9. The L_c, Lam, and PL phases display a weak frequency dependence with comparable values for the storage and loss moduli. The moduli in the gyroid phase display a stronger frequency dependence with a crossover in the storage and loss moduli to a nonterminal regime. The maximum in the loss modulus is characteristic of all cubic phases. At even higher T, at 553 K, the moduli show a terminal behavior with slopes of 1 and 2 for the storage and loss moduli, respectively. On the basis of the isothermal frequency scans alone, it would be difficult to distinguish between the layered structures. However, the combined information from SAXS and isochronal temperature runs of Figure 7 serve this purpose quite well.

Stability of the PL Phase. In subsequent experiments, we examined the stability of the intermediate PL structure. Already, the results in Figure 7 revealed that this structure can be bypassed on cooling from the gyroid phase, which transforms directly to the Lam structure. The corresponding SAXS spectra on cooling from the gyroid phase are shown in Figure 10 and are compared with the spectrum obtained on first heating at the same temperature (333 K). The spectrum taken on cooling shows mixed reflections corresponding to the gyroid and Lam structures, however, the main peak at Q^* is now shifted to higher Q values implying the relief of chain stretching. Upon lowering the temperature, the diblock crystallizes and a second heating experiment results in an identical spectrum to that of the first heating experiment at the same temperature. The combined information from SAXS and rheology together with the absence of endothermic peaks in the vicinity of the Lam to PL and PL to gyroid phases shows that this structure is imposed as an intermediate between the Lam and gyroid purely for kinetic reasons and is not an equilibrium phase and as such should not be included in equilibrium phase diagrams. In our discussion below with respect to the phase state, we chose to show phases which appear on cooling rather than on heating for the two diblock copolymers PEO−PI 7−3 and 9−3 where the PL phase appears.

The reversibility of the PL to gyroid and gyroid to Lam transformations obtained on heating and subsequent cooling of the PEO−PI 7−3 copolymer have been examined and the resulting characteristic transformation temperatures are shown in Figure 11 for different heating and cooling rates. As shown in Figure 11, the forward and backward phase transformations are independent from the heating and cooling rates and the PL to gyroid and gyroid to Lam transitions occur at 496 and 458 K, respectively.

Thermal Expansion of Ordered Phases. Having established the different phases and their stability, we examine next the thermodynamic parameters of thermal expansion and isothermal compressibility associated with each phase. The thermal expansion and isothermal compressibility parameters were extracted from the ln V vs T and ln V vs P representations respectively, and the results for the PEO−PI 7−3 copolymer are shown in Figure 11 together with the (linear) regimes used in extracting the values of α_P. The results show that each phase has a different α_P and that the following approximate relationships hold:

$$\alpha_G > \alpha_{PL} \geq \alpha_{Lam} > \alpha_{L_c} \quad (2)$$

and

$$\beta_G > \beta_{PL} \geq \beta_{Lam} > \beta_{L_c} \quad (3)$$

The values of the thermal expansion coefficient within the L_c, Lam, PL, and gyroid phases are 5.07×10^{-4}, 5.94×10^{-4}, 6.61×10^{-4} and 8.45×10^{-4} K^{-1}, respectively. It is worth noticing the similarity in the thermodynamic properties of the Lam and PL phases (the former is higher by 10%) and the much higher thermal expansion coefficient and isothermal compressibility of the high T phase (gyroid) (22% higher in the gyroid than in the PL phase). These could be compared with the T dependence of the unperturbed chain dimensions $\partial(\ln r_o^2)/\partial T = 2.89 \times 10^{-4}$ K^{-1} (calculated from the corresponding PEO and PI values of 2.3×10^{-4} and 4.1×10^{-4} $K^{-1}$and the block composition[36]). The higher values of the thermal expansion indicate stretching of chains within the ordered domains.

In the same Figure we plot the $Q^*(T)$ dependence of the same copolymer obtained on heating from the L_c phase. The ln Q^* shows a discontinuous increase at the

melting temperature and a sigmoidal shape at higher temperatures. There is a large mismatch between the Q^* of the Lam and gyroid structures and the strong increase of Q^* within the PL phase implies that this phase serves to provide the needed intermediate length scale for the Lam to gyroid transformation. The $Q^*(T)$ is similar to that for the poly(ethylene oxide-*b*-ethyl ethylene) (PEO−PEE)[37] and poly(oxyethylene-*b*-oxybutylene) (PEO−PBO)[38] diblock copolymer systems. The calculated d(ln Q^*)/dT values within the Lam and PL phases are estimated as 1.2×10^{-3} and 2.9×10^{-3} K^{-1} and are 2 and 4 times higher, respectively, than the corresponding coefficients of thermal expansion. On the basis of $Q^*(T)$ and the values of the thermal expansion coefficient within the Lam and PL phases, we calculate the increase of the area per copolymer junction at the interface based on simple geometrical considerations.[39] In our calculation, we have assumed that the area per junction within the PL phase can be expressed as a weighted average from the Lam and Hex phases. We find that within the Lam and PL phases, over a T range of 50 K, the areas per junction increase by 12 and 20 Å^2, respectively. In conclusion, the $Q^*(T)$ and α dependencies suggest a large increase of the area per junction within the intermediate PL phase.

Phase Diagram. The complete phase behavior requires knowledge of the temperature dependence of χ. One way to obtain $\chi(T)$ is from the T_{ODT} in copolymers with the same composition but different molecular weights by using the MFT prediction for the (χN) at the spinodal or to the corresponding value suggested by the fluctuation approach. However, this method requires diblocks of the same composition but of very different molecular weights, with well separated transition temperatures. For the PEO−PI system, the N values are low and preclude this type of analysis. We have used, instead, the χ(T) obtained previously[26] ($\chi = 65/T + 0.125$) by fitting the disordered phase structure factor of the PEO−PI 1−5 copolymer to the MFT predictions. This $\chi(T)$ results in a higher value when compared to other known systems (i.e., $\chi_{PE-PEE} = 15/T - 0.0055$,[40] $\chi_{PS-PI} = 71/T - 0.086$,[41] $\chi_{PS-P2VP} = 92/T - 0.095$,[42] $\chi_{PE-PEP} = 4.7/T + 0.00044$,[43] $\chi_{PEO-PBO} = 48.5/T - 0.05$[44] where PE, PEE, P2VP, PEP, and PBO stand for polyethylene, poly(ethyl ethylene), poly-2-vinylpyridine, poly(ethylene propylene), and poly(butylene oxide)). Using this $\chi(T)$ and the transition temperatures from Table 1 results in the phase diagram shown in Figure 13. In Figure 13, only equilibrium phases are shown; i.e., the PL phase, based on our discussion, is excluded. Thus, the phase diagram is composed of five phases in equilibrium (here we refer to the crystalline lamellar as an equilibrium phase): The L_c dominates the phase behavior at intermediate and strong segregations. The Lam phase has a peculiar appearance owing to the L_c formation at intermediate segregation. The gyroid phase is found from both sides of the phase diagram being the last phase before disordering. The Hex phase for some volume fractions has a direct access to the disordered state. Because of the asymmetric compositions employed here, the bcc phase was only found on one side of the phase diagram. The phase diagram allows for direct transitions between the Hex and gyroid phases for $0.38 < f_{PEO} < 0.46$ and between the Lam and gyroid on cooling diblocks with compositions in the range $0.66 < f_{PEO} < 0.7$.

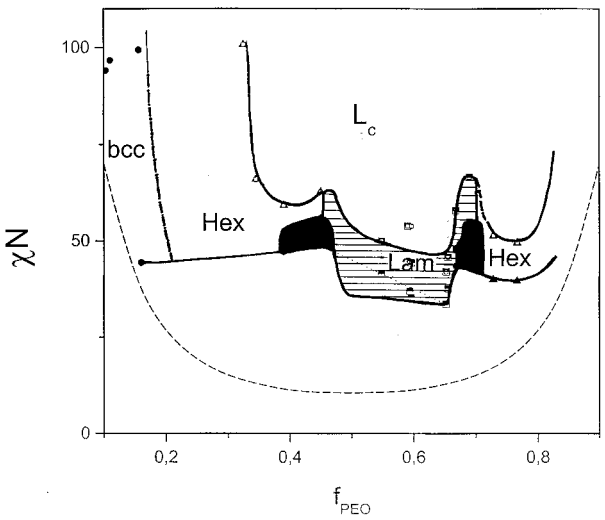

Figure 13. Phase diagram for the system PEO−PI comprising all samples from Table 1. The phase notation is as follows: L_c, crystalline lamellar, Lam, amorphous lamellar, Hex, hexagonal packed cylinders, G, bicontinuous cubic structure with $I\alpha\bar{3}d$ space group symmetry (gyroid-shadowed areas) Only the equilibrium phases are shown which are obtained on cooling from high temperatures (notice the absence of the PL phase). The ODT and OOT temperatures were identified by SAXS and rheology. Values of χN were obtained by using $\chi = 65/T + 0.125$.[26] The dashed line gives the spinodal line in the mean-field prediction. Notice the pronounced asymmetry of the phase diagram with ordered phases shifted parallel to the composition axis. The asymmetric appearance can be accounted for by the conformational asymmetry of the segments (see text).

These findings for the PEO−PI system can be compared with other known systems. The most extensively studied system is the PI−PS.[5,41] Other systems, such as PE-PEE, PS−P2VP, PEP−PEE, and PEO−PBO, have also been studied but with less accuracy (about 20 copolymers are needed with appropriate compositions for the construction of a phase diagram). The PEO−PI phase diagram shows many similarities to the PI−PS system but less to the other systems investigated. On the basis of these early phase diagrams, it has been suggested, that apart from χN and f, there exist two additional parameters which influence the shape and relative position of phases, namely, the conformational asymmetry, ϵ, and the fluctuation effects (scaling as $\bar{N}^{-1/3}$). They are responsible, respectively, for the asymmetric overall appearance and stability of the gyroid phase. The PEO−PI system exhibits the highest conformational asymmetry parameter, $\epsilon = 2.72$ (in the calculation we have used, $\alpha_{PI} = 0.59$ nm, $\alpha_{PEO} = 0.7$ nm, $u_{PI} = 0.126$ nm^3 and $u_{PEO} = 0.065$ nm^3). This value should be compared with $\epsilon_{PS-P2VP} \approx 1$, $\epsilon_{PI-PS} = 1.5$, $\epsilon_{PEP-PEE} = 1.7$, and $\epsilon_{PE-PEE} = 2.5$.[25] In these systems the gyroid phase was obtained for $0.35 < f_{PS} < 0.4$, $0.35 < f_{PI} < 0.4$, $0.38 < f_{PEP} < 0.42$, and $0.37 < f_{PE} < 0.43$. It is the first time that a gyroid structure is observed for $0.4 < f_{PEO} < 0.45$, i.e., for such high volume fractions of the minority component. Clearly, conformational asymmetry plays a dominant role in shifting the phase diagram parallel to the composition axis in agreement with the earlier studies, however, the absence of the gyroid phase for $f > 0.5$ in the PE-PEE and PEP−PEE systems[25] cannot be attributed to conformational asymmetry but rather to the incompleteness of the phase diagram.

The effect of fluctuations is also of importance in the present system. In the evaluation of $\bar{N}$ we have used a nearly symmetric sample ($f_{PEO} = 0.45$, $T_{ODT} = 503$ K) and calculated the effective segment length as $\alpha^2 = f_{PEO}\alpha_{PEO}^2 + f_{PI}\alpha_{PI}^2$. Using an average segment volume $u = 91$ Å^3 we obtain $N = 1.6 \times 10^3$ whereas the previously employed segment volume from different systems[25] of 118 Å^3 results in $\bar{N} = 0.96 \times 10^3$. The latter is the lowest value among the known phase diagrams and suggests strong fluctuation effects which shift the phase diagram parallel to the χN axis and possibly stabilize the gyroid phase.

IV. Conclusions

The phase diagram of the PEO−PI system has been constructed based on 25 diblock copolymers spanning the composition range $0.05 < f_{PEO} < 0.8$. Five ordered phases have been identified based on their scattering patterns and viscoelastic properties: crystalline lamellar, amorphous lamellar, cylinders packed in a hexagonal lattice, spheres in a bcc lattice, and a phase with the $Ia\bar{3}d$ space group symmetry known as the gyroid. In addition, a perforated layered structure was found which facilitates the Lam to gyroid forward transformation. The PL phase, however is absent on cooling and therefore is not an equilibrium phase and as such was not included in our phase diagram. The phase diagram allows for direct transitions between the Hex and gyroid phases for $0.38 < f_{PEO} < 0.46$ and between the Lam and gyroid on cooling diblocks with compositions in the range $0.66 < f_{PEO} < 0.7$.

The present system has a high interaction parameter, a low N and the highest value of the conformational asymmetry ($\epsilon = 2.72$) reported so far. We found that the phase diagram is shifted along the composition axis toward the component possessing the more asymmetric segments. As a result, the gyroid structure is observed for $0.4 < f_{PEO} < 0.45$, with the upper bound being the highest composition ever reported. The thermal expansion coefficient was found to be a sensitive probe of the ordered microstructures.

Recently,[45,46] it was shown that the combination of the present PEO−PI diblock copolymers with organically modified ceramic precursors (ormocers) allows for a rational organic−inorganic hybrid morphology design. This leads to unprecedented structural control of the resulting nanostructured materials. In future studies of such polymer-inorganic hybrid materials based on PEO−PI block copolymers as structure directing agents, we will use the knowledge of the present phase diagram aiming to construct a quasi-ternary phase diagram with the inorganic precursors.

Acknowledgment. G.F. acknowledges Prof. T. Pakula for discussions, Mr. A. Best for the *PVT* measurements and the MPI-P for its hospitality. We thank A. DuChesne for the TEM study. The financial support to G.F. by the Empeirikeion Foundation and by IESL-FORTH (internal grant) is gratefully acknowledged. G.F. and U.W. acknowledge the European Union TMR network (ERBFMRXCT970112) for support and discussions with the "CAPS" group members. U.W. acknowledges the financial support of the NSF (Grant DMR-0072009), the Cornell Center for Materials Research (CCMR) and the Materials Research Science and Engineering Center of the NSF (DMR-0079992).

References and Notes

(1) Bates, F. S.; Fredrickson, G. H. *Phys. Today* **1999**, 32−38.
(2) Hamley, I. *The Physics of Block Copolymers*; Oxford University Press: Oxford, U.K., 1998.
(3) Callejia, F. J. B., Roslaniec, Z., Eds. *Block Copolymers*, Marcel Dekker: New York, 2000.
(4) Leibler, L. *Macromolecules* **1980**, *13*, 1602.
(5) Förster, S.; Khandpur, A. K.; Zhao, J.; Bates, F. S.; Hamley, I.; Ryan, A. J.; Bras, W. *Macromolecules* **1994**, *27*, 6922.
(6) Hajduk, D. A.; Takenouchi, H.; Hillmyer, M. A.; Bates, F. S.; Vigild, M. E.; Almdal, K. *Macromolecules* **1997**, *30*, 3788.
(7) Vigild, M. E.; Almdal, K.; Mortensen, K.; Hamley, I. W.; Fairclough, J. P. A.; Ryan, A. J. *Macromolecules* **1998**, *31*, 5702.
(8) Hajduk, D. A.; Harper, P. E.; Gruner, S. M.; Honeker, C. C.; Kim, G.; Thomas, E. L.; Fetters, L. J. *Macromolecules* **1994**, *27*, 4063.
(9) Olvera de la Cruz, M.; Sanchez, I. C. *Macromolecules* **1986**, *19*, 2501.
(10) Floudas, G.; Hadjichristidis, N.; Iatrou, H.; Pakula, T.; Fischer, E. W. *Macromolecules* **1994**, *27*, 7735.
(11) Floudas, G.; Pispas, S.; Hadjichristidis, N.; Pakula, T.; Erukhimovich, I. *Macromolecules* **1996**, *29*, 4142.
(12) Floudas, G.; Hadjichristidis, N.; Tselikas, Y.; Erukhimovich, I. *Macromolecules* **1997**, *30*, 3090.
(13) Floudas, G.; Hadjichristidis, N.; Iatrou, H.; Avgeropoulos, A.; Pakula, T. *Macromolecules* **1998**, *31*, 6943.
(14) Hodrokoukes, P.; Floudas, G.; Pispas, S.; Hadjichristidis, N. *Macromolecules* **2001**, *34*, 650.
(15) Pochan, J.; Gido, S. P.; Pispas, S.; Mayes, J. W.; Ryan, A. J.; Fairclough J. P. A.; Hamley, I. W.; Terrill, N. J. *Macromolecules* **1996**, *29*, 5091.
(16) Xenidou, M.; Beyer, F. L.; Hadjichristidis, N.; Gido, S. P.; Tan. N. B. *Macromolecules* **1998**, *31*, 7659.
(17) Pochan, D. J.; Gido, S. P.; Pispas, S.; Mays, J. W. *Macromolecules* **1996**, *29*, 5099.
(18) Fredrickson, G. H.; Helfand, E. *J. Chem. Phys.* **1987**, *87*, 697.
(19) Erukhimovich, I.; Dobrynin, A. V. *Macromol. Symp.* **1994**, *81*, 253.
(20) Vavasour, J. D.; Whitmore, M. D.; *Macromolecules* **1993**, *26*, 7070; **1996**, *29*, 5244.
(21) Matsen, M. W.; Schick, M. *Macromoleucles* **1994**, *27*, 4014.
(22) Matsen, M. W.; Bates, F. S. *J. Polym. Sci., Polym. Phys.* **1997**, *35*, 945.
(23) Rosedale, J. H.; Bates, F. S.; Almdal, K.; Mortensen, K.; Wignall, G. D. *Macromolecules* **1995**, *28*, 1429.
(24) Zhao, J.; Majumdra, B.; Schulz, M. F.; Bates, F. S.; Almdal, K.; Mortensesn, K.; Hajduk, D. A.; Gruner, S. M. *Macromolecules* **1996**, *29*, 1204.
(25) Bates, F.; Schulz, M. F.; Khandpur, A. K.; Förster, S.; Rosedale, J. H.; Almdal, K.; Mortensen, K. *Faraday Discuss., Chem. Soc.* **1994**, *98*, 7.
(26) Floudas, G.; Ulrich, R.; Wiesner, U. *J. Chem. Phys.* **1999**, *110*, 652.
(27) Floudas, G.; Ulrich, R.; Wiesner, U.; Chu, B. *Europhys. Lett.* **2000**, *50*, 182.
(28) Hadjichristidis, N.; Iatrou, H.; Pispas, S.; Pitsikalis, M. *J. Polym. Sci., Polym. Chem.* **2000**, *38*, 3211.
(29) Esswein, B.; Möller, M. *Angew. Chem., Int. Ed. Engl.* **1996**, *35*, 623.
(30) Förster, S.; Kramer, E. *Macromolecules* **1999**, *32*, 2783.
(31) Schipper, F.; Floudas, G. Manuscript in preparation.
(32) Van Krevelen, D. W. *Properties of Polymers*, 2nd ed.; Elsevier: Amsterdam, 1976.
(33) Hajduk, D. A.; Gruner, S. M.; Erramilli, S.; Register, R. A.; Fetters, L. J. *Macromolecules* **1996**, *29*, 1473.
(34) Floudas, G.; Hadjichristidis, N.; Stamm, M.; Likhtman, A. E.; Semenov, A. N. *J. Chem. Phys.* **1997**, *106*, 3318.
(35) Floudas, G.; Pakula, T.; Velis, G.; Sioula, S.; Hadjichristidis, N. *J. Chem. Phys.* **1998**, *108*, 6498.
(36) Brandrup, J., Immergut, E. H., Eds. *Polymer Handbook*, 2nd ed.; Interscience: New York, 1975.
(37) Hillmyer, M. A.; Bates, F. S.; Almdal, K.; Mortensen, K.; Ryan, A. J.; Fairclough *Science* **1996**, *271*, 976.
(38) Hamley, I. W.; Fairclough, J. P. A.; Ryan, A. J.; Mai, S.-M.; Booth, C. *Phys. Chem. Chem. Phys.* **1999**, *1*, 2097.
(39) Winey, K. I.; Thomas, E. L.; Fetters, L. J. *J. Chem. Phys.* **1991**, *95*, 9367.

(40) Bates, F. S.; Schultz, M. F.; Rosedale, J. H.; Almdal, K. *Macromolecules* **1992**, *25*, 5547.
(41) Khandpur, A. K.; Förster, S.; Bates, F. S.; Hamley, I. W.; Ryan, A. J.; Bras, W.; Almdal, K.; Mortensen, K. *Macromolecules* **1995**, *28*, 8796.
(42) Schulz, M. F.; Khandpur, A. K.; Bates, F. S.; Almdal, K.; Mortensen, K.; Hajduk, D. A.; Gruner, S. M. *Macromolecules* **1996**, *29*, 2857.
(43) Rosedale, J. H.; Bates, F. S. *Macromolecules* **1990**, *23*, 2329.
(44) Mai, S.-M.; Fairclough, J. P. A.; Hamley, I. W.; Matsen, M. W.; Denny, R. C.; Liao, B.-X.; Booth, C.; Ryan, A. J. *Macromolecules* **1996**, *29*, 6212.
(45) Templin, M.; Franck, A.; DuChesne, A.; Leist, H.; Zhang, Y.; Ulrich, R.; Schadler, V.; Wiesner, U. *Science* **1997**, *278*, 1795.
(46) Ulrich, R.; DuChesne, A.; Templin, M.; Wiesner, U. *Adv. Mater.* **1999**, *2*, 141.

MA001957P